33. BASALTS FROM DEEP SEA DRILLING PROJECT HOLES 417A AND 417D, FRACTIONATED MELTS OF A LIGHT RARE-EARTH DEPLETED SOURCE

S. Rice, C. H. Langmuir, J. F. Bender, G. N. Hanson, and A. E. Bence,
Department of Earth and Space Sciences, State University of New York, Stony Brook, New York
and
S. R. Taylor, Research School of Earth Sciences, Australia National University, Canberra, ACT 2600, Australia

ABSTRACT

Tholeiitic basalts from DSDP Holes 417A and 417D consist of two textural types: phyric and subophitic. Their major element and transition metal spectra are a consequence of the low-pressure fractionation of olivine prior to emplacement, and plagioclase accumulation during or after emplacement. Reverse, normal, and oscillatory zoning of the plagioclase phenocrysts within the same sample suggests magma mixing. Incompatible element abundances suggest a chemically and mineralogically homogeneous source region depleted in the light rare earth elements (LREE) relative to the heavy rare earth elements (HREE). Alteration of some samples has significantly affected the abundances of SiO_2, MgO, K_2O, H_2O, and Fe_2O_3. Alumina and titania are relatively immobile, with reference to the fresh basalts, in the one highly altered sample which was analyzed. No REE fractionation is observed.

INTRODUCTION

The primary objective of drilling at Site 417 during DSDP Legs 51 and 52 was deep penetration of the Cretaceous oceanic crust at 25°N, 68°W. On Leg 51, a pilot hole (417A) penetrated 206 meters of basement. A second hole (417D) was started nearby, and was re-entered on Leg 52. At Hole 417D, 366 meters of basement was penetrated, with recovery of about 270 meters of basalts.

From mineralogical and apparent contact relationships, 14 units of pillow lavas and massive flows, and 1 small dike were recognized in the sequence recovered in Hole 417D (Site 417 Report, this volume). Most of these units are represented in our samples, which include 2 glasses and 30 crystalline basalts from pillows and massive flows. The crystalline rocks range from very fresh to extensively altered.

This paper presents the results of a major element, trace element, and phase chemical investigation of 22 crystalline basalts from both holes. The objectives of this investigation are to accomplish the following: (1) compare these basalts with those from other DSDP sites; (2) document variations within a thick, ancient ocean crustal sequence; (3) assess the effects of alteration on selected major and trace elements; and (4) generate models for the origin and evolution of these basalts.

If these basalts are the products of mid-ocean ridge (MOR) volcanism, comparisons can be made with both younger and older basalts generated at the same ridge to document the time dependence of MORB chemistry. Holes 417A and 417D lie near the eastern edge of magnetic anomaly *M*0 (Site 417 Report, this volume), and are inferred to be 109×10^6 years old. These holes lie along the same spreading line as the slightly older Leg 11, Site 100 basalts (Ayuso et al., 1977), and the very young (about 7×10^6 years) basalts from Sites 395 and 396 of DSDP Leg 45, located near the crest of the Mid-Atlantic Ridge.

ANALYTICAL TECHNIQUES

Major element bulk chemical analyses (Table 1) of 21 glass beads fused from powders on an iridium strip furnace (Nicholls, 1974) were obtained on an automated ARL-EMX-SM electron microprobe at Stony Brook. Reduction procedures for these and the phase chemical data are modifications of those of Bence and Albee (1968). Basalt standards BCR-1 and BHVO-1 prepared in the same manner as the unknowns were used to monitor the glass analyses.

REE abundances (Table 2) for three basalts from Holes 417A and 417D were determined at Stony Brook using isotope dilution, and were analyzed on an automated 12-inch NBS design mass spectrometer (Hanson, in preparation). The abundances of the REE, Th, U, Zr, Hf, Nb, Ba, and Pb in these samples were determined by spark source mass spectrometry at the Australian National University (ANU) using the technique described by Taylor and Gorton (1977).

The abundances of the transition metals Cr, V, Sc, Co, Ni, and Cu were determined by emission spectroscopy at ANU, using the technique of Ahrens and Taylor (1961), and are reported in Table 2. Monitors for these elements included W-1, BCR-1, and BHVO-1.

MODAL MINERALOGY, PETROGRAPHY, AND PHASE CHEMISTRY

The basalts from Holes 417A and 417D are represented by two petrographic types: a fine-grained variety containing phenocrysts and microphenocrysts of plagioclase, olivine

TABLE 1
Major Element Analyses and Normative Mineralogy, Holes 417A and 417D

	1	2	3	4	5	6	7	8	9	10	11	12	13	14	15	16	17	18	19	20	21	22	23
SiO_2	49.1	49.7	49.2	48.7	50.0	50.2	46.6	48.8	48.0	49.8	49.3	49.6	49.1	48.6	49.1	49.6	49.7	49.8	49.7	50.1	47.8	49.8	48.7
TiO_2	1.36	1.56	1.53	1.59	1.52	1.50	1.35	1.43	1.44	1.63	1.55	1.46	1.68	1.44	1.61	1.46	1.47	1.40	1.43	1.34	1.33	1.49	1.78
Al_2O_3	17.0	14.4	17.9	15.8	14.2	16.7	15.1	17.6	17.1	15.6	17.2	15.0	17.4	14.5	15.7	16.9	16.8	17.4	16.5	16.0	15.3	16.7	20.6
Cr_2O_3	–	0.03	0.04	0.04	0.04	0.04	0.02	0.04	0.04	0.02	0.04	0.01	0.02	0.02	0.04	0.03	0.03	0.04	0.03	0.01	–	–	0.01
Fe_2O_3	1.12	1.33	1.08	1.35	1.33	1.13	1.15	1.18	1.17	1.38	1.23	1.46	1.15	1.68	1.32	1.25	1.08	1.17	1.21	1.20	1.23	1.22	–
FeO	8.09	9.63	7.82	9.73	9.58	8.14	8.31	8.54	8.42	9.95	8.87	10.56	8.32	12.15	9.52	9.04	7.80	8.42	8.76	8.66	8.48	8.80	13.5
MnO	0.13	0.17	0.18	0.18	0.17	0.15	0.15	0.16	0.16	0.10	0.16	0.13	0.12	0.09	0.18	0.17	0.19	0.16	0.19	0.14	0.18	0.16	0.14
MgO	6.47	7.77	6.00	6.78	7.79	6.29	5.96	6.22	6.37	6.92	6.75	6.97	7.40	7.22	6.68	6.25	6.28	6.86	6.90	7.32	9.41	6.76	2.36
CaO	12.9	11.6	13.3	12.8	11.7	12.6	18.1	13.3	13.6	10.8	12.2	10.5	11.4	10.1	12.7	13.1	13.1	12.3	12.7	12.5	12.0	12.4	5.24
Na_2O	2.44	2.39	2.52	2.42	2.37	2.44	2.30	2.44	2.36	2.37	2.59	2.20	2.67	2.30	2.27	2.27	2.49	2.22	2.10	2.27	2.00	2.16	2.42
K_2O	0.76	0.13	0.24	0.26	0.12	0.11	0.27	0.22	0.16	0.72	0.39	0.97	0.09	1.04	0.25	0.06	0.10	0.10	0.05	0.06	0.06	0.10	3.94
Σ	99.4	98.7	99.8	99.7	98.9	99.3	99.4	100.0	98.8	99.3	100.2	98.9	99.3	99.1	99.4	100.2	99.0	99.9	99.6	99.6	98.1	99.7	98.7
$Mg/(Mg + Fe^{2+})$	0.59	0.59	0.58	0.55	0.59	0.58	0.56	0.56	0.57	0.55	0.58	0.54	0.61	0.51	0.56	0.55	0.59	0.59	0.58	0.60	0.65	0.58	0.26
AB	20.65	20.22	21.32	20.48	20.05	20.65	18.62	20.65	19.97	20.05	21.92	18.62	22.59	19.46	19.21	19.21	21.07	18.79	17.77	19.21	16.92	18.28	20.48
AN	33.27	28.32	36.88	31.40	27.75	34.29	28.30	36.39	35.59	29.75	34.05	28.30	35.17	26.11	31.99	35.83	34.29	37.35	35.50	33.29	32.59	35.58	26.00
OR	4.49	0.77	1.42	1.54	0.71	0.65	5.73	1.30	0.95	4.25	2.30	5.73	0.53	6.15	1.48	0.35	0.59	0.59	0.30	0.35	0.35	0.59	23.28
OL	11.05	3.55	7.03	9.77	2.43	0.31	5.30	9.22	10.28	4.70	10.15	5.30	7.95	12.64	5.36	2.72	3.22	1.87	0.39	1.99	10.37	–	10.42
FA	4.97	1.59	3.19	4.74	1.09	0.14	2.67	4.36	4.75	2.27	4.67	2.67	3.28	6.73	2.58	1.33	1.43	0.83	0.18	0.88	4.00	–	8.04
FO	6.09	1.95	3.85	5.03	1.35	0.17	2.63	4.86	5.53	2.43	5.48	2.63	4.67	5.89	2.78	1.39	1.79	1.03	0.21	1.12	6.37	–	2.38
PYR	25.75	40.92	28.64	31.46	43.09	38.91	36.07	27.97	27.49	35.43	27.04	36.07	28.17	29.49	36.30	37.46	35.42	36.88	41.11	40.48	33.45	40.07	10.04
DI	25.17	23.78	23.69	26.54	25.01	23.33	19.59	24.52	26.12	19.69	21.84	19.59	17.36	19.75	25.47	23.97	25.22	19.42	22.43	23.58	21.26	20.12	–
HY	0.58	17.14	4.95	4.92	18.07	15.58	16.48	3.46	1.38	15.74	5.20	16.48	10.81	9.74	10.83	13.49	10.20	17.46	18.68	16.90	12.19	19.95	10.04
XIL	2.58	2.96	2.91	3.02	2.89	2.85	2.77	2.72	2.73	3.10	2.94	2.77	3.19	2.73	3.06	2.77	2.79	2.66	2.72	2.54	2.53	2.83	3.38
XMT	1.63	1.93	1.57	1.96	1.93	1.64	2.12	1.71	1.69	2.00	1.78	2.12	1.67	2.44	1.91	1.82	1.57	1.69	1.76	1.74	1.78	1.77	2.41
CR	–	0.04	0.06	0.06	0.06	0.06	0.01	0.06	0.06	0.03	0.06	0.01	0.03	0.03	0.06	0.04	0.04	0.06	0.04	0.01	–	–	0.01
Q	–	–	–	–	–	–	–	–	–	–	–	–	–	–	–	–	–	–	–	–	–	0.20	–
COR	–	–	–	–	–	–	–	–	–	–	–	–	–	–	–	–	–	–	–	–	–	–	2.83

Note: Column 1: 417D-26-6, 135-140 cm; Column 2: 417D-26-6, 135-140 cm, natural glass; Column 3: 417D-26-5, 74-81 cm; Column 4: 417D-28-6, 104-110; Column 5: 417D-29-6, 1-6 cm, natural glass; Column 6: 417D-31-2, 93-97 cm; Column 7: 417D-32-2, 27-33 cm; Column 8: 417D-35-4, 11-16 cm; Column 9: 417D-39-4, 84-90 cm; Column 10: 417D-42-6, 97-102 cm; Column 11: 417D-43-3, 36-42 cm; Column 12: 417D-44-1, 60-66 cm; Column 13: 417D-44-4, 80-85 cm; Column 14: 417D-50-1, 57-59 cm; Column 15: 417D-55-5, 110-112 cm; Column 16: 417D-64-1, 80-82 cm; Column 17: 417D-68-2, 67-69 cm; Column 18: 417A-44-2, 8-13 cm; Column 19: 417A-43-5, 8-13 cm; Column 20: 417A-44-4, 5-8 cm; Column 21: 417A-46-1, 23-28 cm; Column 22: 417A-44-3, 58-68 cm; Column 23: 417A-24-2, 72-75 cm. Ferric iron calculated assuming $Fe^{3+} / (Fe^{3+} + Fe^{2+}) = 0.1$. Analyses 21 and 22 taken from unpublished data of Donnelly.

TABLE 2
Trace Element Abundances (ppm), Holes 417A and 417D

	417A-24-2, 72-75 cm		417A-44-2, 8-13 cm		417A-44-3, 58-68 cm	417D-28-6, 104-110 cm		417D-43-3, 36-42 cm	417D-68-2, 67-69 cm
	ANU	SB	ANU	SB	ANU	ANU	SB	ANU	ANU
La	2.92	–		2.20	2.13	1.88	2.18		
Ce	8.63	9.12		7.10	8.40	8.06	7.19		
Pr	1.72	–		–	1.32	1.20	–		
Nd	10.2	10.08		7.89	7.75	7.21	7.40		
Sm	3.67	3.69		–	2.69	2.58	2.92		
Eu	1.42	1.37		–	0.98	0.98	1.12		
Gd	4.98	5.15		4.25	4.11	3.77	4.05		
Tb	0.96	–		–	0.75	0.71	–		
Dy	6.58	6.70		5.33	5.03	4.62	5.26		
Ho	1.51	–		–	1.16	1.11	–		
Er	4.50	4.38		3.40	3.38	3.20	3.33		
Tm	(0.67)	–		–	(0.48)	0.45	–		
Yb	4.88	4.15		3.24	3.34	3.15	3.19		
La/Yb	0.59	–		0.68	0.64	0.60	0.68		
Th	0.11				0.08	0.12			
U	0.20				–	–			
Zr	64				85	57			
Hf	2.30				2.1	2.04			
Nb	1.6				1.1	1.1			
Ba	115				8.4	7.6			
Pb	2.0				0.83	1.9			
Sc	47		46			49		52	41
V	210		370			460		420	375
Cr	365		390			370		305	255
Co	42		40			49		54	39
Ni	64		78			112		110	64
Cu	90		108			128		98	93

relicts, and clinopyroxene (Plate 1, Figure 1); in a groundmass dominated by clinopyroxene and plagioclase (phyric basalts); and a coarser ophitic to subophitic type (Plate 1, Figure 2). The phyric basalts are further subdivided into two groups on the basis of their phenocryst assemblage: plagioclase-olivine and plagioclase-olivine-clinopyroxene.

Large variations in the modal proportions of total plagioclase and pyroxene are observed in the basalts from Hole 417D (Figure 1, Table 3), but there is no apparent correlation with depth. High modal plagioclase tends to be associated with the ophitic samples, whereas pyroxene tends to be most abundant in phyric samples where it occurs largely in the groundmass. In general, there is a negative correlation of the modal abundances of plagioclase with pyroxene in Hole 417D basalts. Matrix content, a good indicator of the crystallinity and hence cooling rate of the rock, is negatively correlated with modal opaques (largely titanomagnetite) which appear late in the paragenetic sequence of the subophitic basalts. Modal relict olivine is nearly constant (about 2%) throughout the core, except for Samples 417D-39-4, 84 cm and 417D-67-5, 111 cm which have higher abundances (7.3 and 4.7%, respectively).

Phyric Basalts

The phyric basalts frequently contain large (2 to 8 mm) rounded plagioclase phenocrysts which have homogeneous calcic (An_{83}-An_{87}) cores and less calcic (An_{65}-An_{72}) rims (Table 4). Oscillatory and reverse zoning trends are occasionally observed (Figure 2A). Sample 417D-28-6, 104 cm contains plagioclase with all three types of compositional zoning (normal, reverse, and oscillatory); on the other hand, vitrophyre Sample 417D-67-5, 111 cm contains homogeneous feldspars as well as feldspars with both normal and reverse zoning trends. These variable zoning trends suggest complicated and variable crystallization histories. Glomerocrysts, which are common in the phyric samples, are aggregates of either plagioclase (An_{68}-An_{77}), or clinopyroxene ($\pm$ olivine relicts) intergrown with tabular plagioclase (Plate 1, Figures 3 and 4). The plagioclase glomerocrysts often contain individual crystals which are strained and broken. Groundmass plagioclase (An_{40}-An_{65}) occurs as lathlike, skeletal, and swallow-tailed crystals in the vitrophyres. These laths often display a preferred orientation.

Clinopyroxene occurs as phenocrysts/xenocrysts, glomerocryst aggregates, and groundmass grains in the phyric basalts. Major element compositions of the phenocrysts/xenocrysts and glomerocrysts are relatively restricted ($Wo_{35-41}En_{44-54}Fs_{8-16}$; others about 11%) relative to the more iron-rich groundmass pyroxenes (Table 5) and are comparable to the magnesian clinopyroxenes found in other MORBs. The crystallization trend for a zoned clinopyroxene phenocryst in phyric basalt (Sample 417D-50-1, 57 cm) is shown in Figure 2A. The first clinopyroxene to crystallize is enriched in CaO, MgO, and Cr_2O_3. As crystallization proceeds, CaO drops off, then increases; MgO continuously decreases. These changes are accompanied by a very rapid decrease in Cr_2O_3 and a gradual increase in TiO_2. Alumina increases at first, but then decreases as the ferrosilite content increases above about Fs_{25}.

Euhedral relicts after olivine, presently filled with calcite or smectite, are observed in all of the phyric basalts. Olivine appears to have been a near-liquidus phase in these basalts. Fine-grained, granular, titanomagnetite, the last primary phase to crystallize, is disseminated throughout the ground-

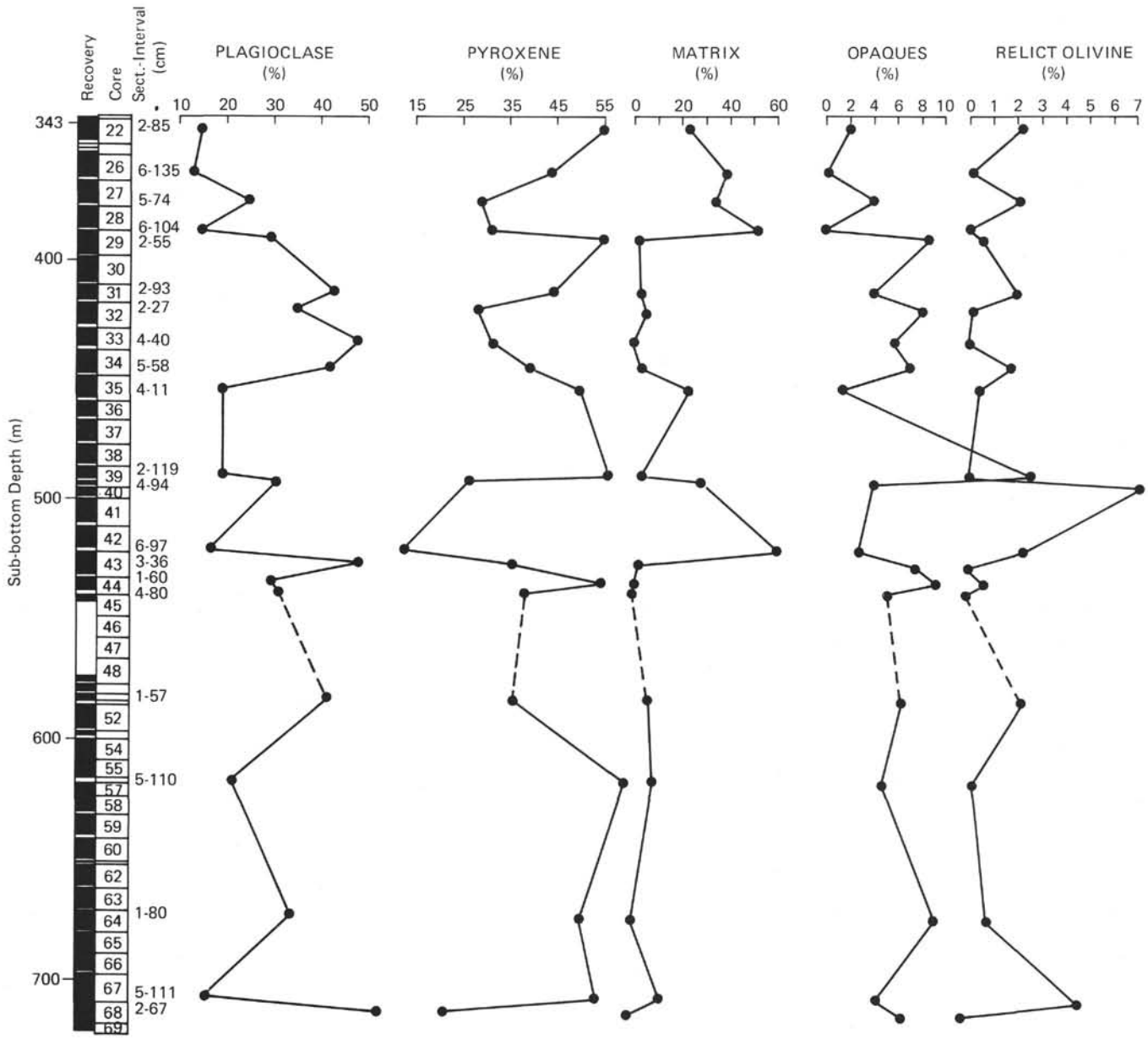

Figure 1. *Modal mineralogical variations in Hole 417D basalts.*

mass in the phyric basalts. Its fine grain size precludes analysis by conventional microprobe techniques.

Subophitic Basalts

The subophitic basalts are dominated by large (up to 2 mm) clinopyroxene oikocrysts partially enclosing plagioclase laths and surrounded by a fine-grained, intersertal matrix of plagioclase, clinopyroxene, titanomagnetite, and glass (now altered to clay minerals). Olivine (Fo_{86}-Fo_{82}) (Table 6) is present in only one of the subophitic basalts (Sample 417A-46-1, 23 cm), where it is partially serpentinized. Its former presence in all other samples is indicated by euhedral relicts now containing calcite or smectite. Basalt Sample 417A-46-1, 23 cm also contains chromian spinel (Table 7) adjacent to the olivine. Spinel and olivine may have been co-liquidus phases.

Rare plagioclase phenocrysts in this textural group have cores as calcic as An_{91} and are zoned to about An_{60} rims. Interstitial plagioclase is as sodic as Ab_{85} (Table 4).

In both textural groups, the early crystallizing feldspars contain low "FeO" (about 0.75 wt.%). As the albite component increases with crystallization, the concentrations of both "FeO" and MgO increase until the plagioclase is about An_{60}. At this stage, MgO drops off drastically, while "FeO" continues to increase. These minor element trends, which have been reported by others (e.g., Ayuso et al., 1976; Mazullo and Bence, 1976; Bence et al., 1975; Bryan, 1974), appear to be characteristic of ocean floor basalt plagioclase.

The initial clinopyroxene to crystallize in the subophitic basalts (Table 5, column 13) is a subcalcic augite enriched in Al_2O_3 and Cr_2O_3 (about $Wo_{42}En_{52}Fs_7$; others 10%). As crystallization proceeds, the pyroxene composition follows

TABLE 3
Modal Mineralogy (%), Holes 417A and 417D

Sample (Interval in cm)	Plagioclase	Pyroxene	Relict Olivine	Opaques	Matrix[a]	Vesicles	Interstitial Clay Minerals[b]	Textural Type
Hole 417D								
22-2, 85-91	14.9	54.6	2.2	2.0	22.9	–	2.1	plag-ol phyric
26-6, 135-140	12.7	43.8	tr	0.1	38.3	1.3	0.6	plag-ol-cpx phyric
27-5, 74-81	25.3	29.1	2.2	4.0	33.1	0.9	2.4	plag-ol phyric
28-6, 104-110	14.6	30.9	tr	–	51.9	1.8	tr	plag-ol-cpx phyric
29-2, 55-61	29.7	54.9	0.5	8.6	2.1	0.6	2.8	plag-ol-cpx phyric
31-2, 93-97	43.0	44.5	2.1	4.0	3.5	tr	0.6	plag-ol-cpx phyric
32-2, 27-33	35.1	28.6	0.2	8.2	5.5	15.2	2.5	ophitic
33-4, 40-46	48.5	31.2	tr	5.7	–	–	2.6	ophitic
34-5, 58-64	42.5	39.3	1.8	7.1	3.4	–	5.2	plag-ol-cox phyric
35-4, 11-16	20.9	50.1	0.5	1.5	23.3	0.3	0.6	plag-ol-cpx phyric
39-2, 119-125	19.8	56.2	tr	17.5	3.2	2.8	0.4	aphanitic
39-4, 84-90	31.1	27.1	7.3	4.2	29.1	2.6	–	plag-ol-cpx phyric
42-6, 97-102	17.7	13.5	2.4	2.9	61.4	0.9	0.8	plag-ol-cpx phyric
43-3, 36-42	49.2	36.6	tr	7.7	3.2	1.0	1.2	plag-ol-cpx phyric
44-1, 60-66	30.6	55.0	0.8	9.6	0.6	0.1	1.3	plag-ol-cpx phyric
44-4, 80-85	32.2	39.2	tr	5.4	0.2	0.1	3.3	plag-ol-cpx phyric
50-1, 57-59	42.4	36.5	2.8	6.7	7.2	–	4.2	plag-ol-cpx phyric
55-5, 110-112	22.5	60.1	0.2	5.0	8.9	0.8	1.1	plag-ol-cpx phyric
64-1, 80-82	35.7	51.0	0.9	9.5	–	–	0.3	plag-ol phyric
67-5, 111-114	17.6	54.9	4.7	4.6	12.3	–	1.7	plag-ol-cpx phyric
68-2, 67-69	54.2	27.8	1.0	6.6	–	0.4	–	ophitic
Hole 417A								
40-2, 130-136	43.9	35.8	1.0	6.1	8.6	tr	0.8	plag-ol-cpx phyric
43-5, 8-13	50.4	33.2	tr	6.0	0.3	tr	4.0	ophitic
44-2, 8-13	43.6	45.8	tr	8.1	–	0.1	1.7	plag-ol-phyric
44-4, 5-8	48.2	27.4	tr	7.1	1.1	1.8	7.0	ophitic
46-1, 23-28	47.8	31.8	2.2[c]	7.0	2.7	–	6.5	ophitic

[a] Matrix is defined as that groundmass material with no birefringence and does not include alteration products.
[b] This category does not include alteration products of olivine or vesicle fillings.
[c] Includes 1.3 per cent fresh olivine.

TABLE 4
Plagioclase From Holes 417A and 417D

	1	2	3	4	5	6	7	8	9	10	11	12	13	14	15
SiO_2	48.6	45.8	51.5	63.0	47.0	50.9	51.1	52.6	54.1	49.9	50.4	48.9	46.6	45.6	56.1
Al_2O_3	32.8	34.2	30.4	21.1	34.2	30.8	30.4	30.2	28.8	31.8	31.3	32.1	34.2	34.9	26.0
FeO	0.57	0.65	0.98	2.09	0.49	0.83	0.79	0.90	1.21	0.73	0.67	0.68	0.55	0.48	1.07
MgO	0.21	0.15	0.40	0.26	0.19	0.28	0.20	0.23	0.21	0.19	0.18	0.18	0.15	0.10	0.08
CaO	16.2	17.7	14.2	2.85	17.0	14.4	14.0	12.7	11.9	15.4	15.0	15.8	17.1	18.5	10.6
Na_2O	2.06	1.36	2.96	9.05	1.87	3.14	3.63	4.00	4.45	2.84	3.17	2.54	1.29	0.96	5.38
K_2O	0.05	0.05	0.07	0.57	0.06	0.06	0.05	0.11	0.08	0.06	0.05	0.05	0.04	0.03	0.09
Σ	100.4	99.8	100.5	98.9	100.8	100.3	100.1	100.6	100.8	100.9	100.7	100.2	99.9	100.6	99.3
Si	2.216	2.116	2.338	2.838	2.145	2.316	2.332	2.374	2.437	2.264	2.289	2.238	2.144	2.093	2.551
Al	1.766	1.862	1.625	1.120	1.842	1.651	1.632	1.608	1.530	1.702	1.676	1.731	1.853	1.888	1.397
Fe	0.022	0.025	0.037	0.076	0.019	0.032	0.030	0.034	0.046	0.028	0.025	0.026	0.021	0.018	0.041
Mg	0.014	0.010	0.027	0.018	0.013	0.020	0.014	0.015	0.014	0.013	0.012	0.012	0.010	0.007	0.005
Ca	0.790	0.878	0.689	0.137	0.830	0.701	0.682	0.612	0.574	0.751	0.728	0.775	0.842	0.912	0.516
Na	0.182	0.122	0.260	0.791	0.166	0.277	0.321	0.350	0.389	0.250	0.280	0.226	0.115	0.085	0.475
K	0.003	0.003	0.004	0.033	0.003	0.004	0.003	0.006	0.005	0.003	0.003	0.003	0.002	0.002	0.005
Total Cations	4.994	5.015	4.981	5.013	5.019	4.999	5.014	5.000	4.995	5.012	5.014	5.010	4.988	5.006	4.990
Ks	0.33	0.27	0.40	3.43	0.34	0.37	0.28	0.65	0.50	0.33	0.30	0.28	0.26	0.19	0.54
Ab	18.7	12.1	27.3	82.3	16.6	28.2	31.9	36.1	40.2	24.9	27.7	22.5	12.0	8.54	47.6
An	81.0	87.6	72.3	14.3	83.1	71.4	67.8	63.2	59.3	74.7	72.0	77.2	87.7	91.3	51.8

Note: Column 1: 417D-28-6, 104-110 cm, phenocryst; Columns 2, 3: 417D-31-2, 93-97 cm, phenocryst core, rim; Column 4: 417D-33-4, 40-46 cm, groundmass; Columns 5, 6: 417D-34-5, 58-64 cm phenocryst core, rim; Column 7: 417D-34-5, 58-64 cm, microphenocryst core; Column 8: 417D-44-1, 60-66 cm; groundmass; Column 9: 417D-44-4, 80-85 cm, groundmass; Column 10: 417D-44-4, 80-85 cm, microphenocryst rim; Columns 11, 12: 417D-64-1, 80-82 cm, microphenocryst core, rim; Column 13: 417D-67-5 111-114 cm, phenocryst core; Column 14: 417A-46-1, 23-28 cm, ophitic core; Column 15: 417A-46-1, 23-28 cm, interstitial quench. Analyses normalized to 8 oxygens.

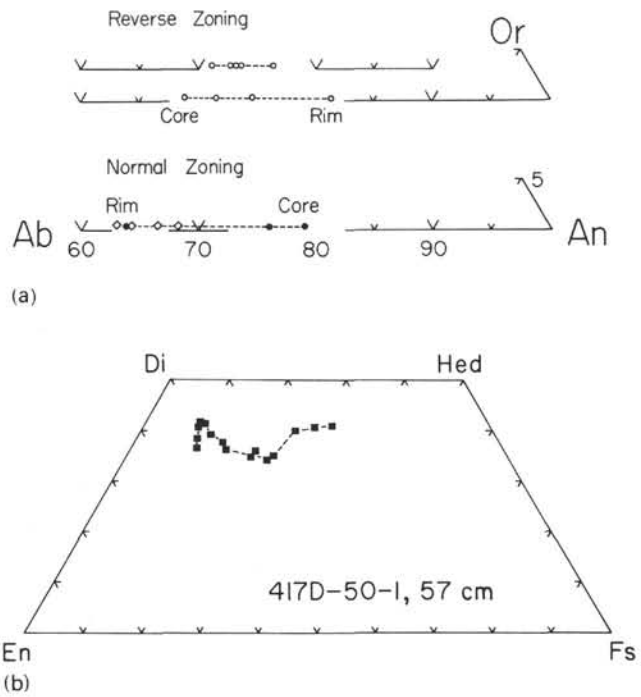

Figure 2. *(A) Normal (solid circle) and reverse (open circle) zoning in plagioclase phenocrysts from plagioclase phyric basalt Sample 417D-64-1, 80 cm. Groundmass plagioclase; diamonds. (B) Zoning in clinopyroxene from phyric basalt Sample 417D-50-1, 57 cm.*

a trend comparable to that observed in Skaergaard calcic pyroxenes (Wager and Brown, 1967).

Oikocryst rims and interstitial pyroxenes are enriched in iron (Table 5, column 14) or depleted in calcium (Table 5, column 15). The low-calcium, high-iron interstitial pyroxenes are enriched in Ti and depleted in Cr and Al relative to the low-Fe oikocrysts. The enrichment in Ti reflects its continual buildup in the residual melt prior to the crystallization of Fe-Ti oxides.

Titanomagnetite (Table 8) in both granular and skeletal forms, is the last phase to crystallize from the melt. Individual grains are compositionally zoned, primarily in the minor elements Al, Mn, Mg, and Cr.

CHEMISTRY

Major Elements

Site 417 basalts are hypersthene-normative and contain 0.30 to 12.6 per cent olivine in the norm (Table 1). The freshest samples have limited ranges of SiO_2 (48.0 to 50.2 wt.%), MgO (6 to 7.4 wt.%), TiO_2 (1.34 to 1.68 wt.%), and atomic $Mg/(Mg + Fe^{2+})$ (0.55 to 0.61) and are typical of other MORBs that have undergone some differentiation.

Chemical variations with core depth among fresh samples are small in Hole 417D (Figure 3) and cannot readily be correlated with modal (Figure 1) or textural variations. Generally increasing SiO_2, MgO, and FeO, and decreasing CaO and Al_2O_3 in the sub-bottom interval from 425 to about 550 meters correlate in part with an increase in the pyroxene/plagioclase ratio, and in part with an increase in the matrix/(pyroxene + plagioclase) ratio.

The extent of alteration as determined petrographically correlates with the K_2O abundances in the basalts from both holes. The content of H_2O (Donnelly, this volume) also shows a positive correlation with the K_2O content. Consequently, the spikes in K_2O abundance in the vertical section (Figure 3) probably reflect regions of extensive alteration. The high CaO content of Sample 417D-32-2, 27-33 cm is due to a high concentration (about 13 modal%) of calcite-filled vesicles. The major components least affected by alteration are Na_2O, Al_2O_3, and TiO_2. Total iron (as FeO) has apparently been introduced from external sources into highly altered Samples 417D-44-1, 60-66 cm and 417D-50-1, 57-59 cm.

Glass Samples 417D-26-6, 135-140 cm and 417D-29-6, 1-6 cm provide an estimate of the composition of the basaltic liquid at the time of emplacement. These glasses have lower Al_2O_3 (about 14 wt. %) and higher MgO (about 7.8%) than the crystalline rocks and plot (Figure 4) in the vicinity of the low-pressure plagioclase-olivine cotectic as determined experimentally for a FAMOUS basalt (Bender et al., in preparation) and inferred from the compositions of abyssal basaltic glasses (Bence et al., in preparation).

Trace Elements

The analyzed basalts from Holes 417A and 417D are progressively depleted in the light REE with $(La/Yb)_N$ ratios of 0.59 to 0.64 (Table 2, Figure 5). Unaltered samples, separated in Hole 417D by as much as 320 meters and numerous cooling units, have virtually identical patterns (Figure 5). Heavy REE abundances range from about 15 to 18 times those observed in chondrites. The REE patterns are generally similar to those of other normal MORBs.

Transition metal abundances for the freshest basalts have a limited range (Table 2, Figure 6). Relative to FAMOUS samples, which probably have undergone minimal differentiation (Langmuir et al., 1977), Hole 417A and 417D basalts are enriched in Sc, Ti, and V, and depleted in Cr and Ni.

Hole 417A and 417D basalts have abundances of U, Th, Zr, Hf, and Nb (Table 2), within the reported range of other LIL-depleted tholeiites (e.g., Frey et al., 1974; Erlank and Kable, 1976). Barium is also low in the unaltered samples.

Alteration

Effects on Major Elements

The basalts recovered in Holes 417A and 417D have a wide range in their degree of alteration, thus permitting an assessment of the mineralogical and chemical effects of alteration in this old segment of the oceanic crust.

Olivine and chrome spinels are the first crystalline phases to break down in response to alteration. They are followed by calcic plagioclase, iron-titanium oxides and, finally, clinopyroxene. New phases generated include serpentine (from olivine), smectite (from glassy groundmass), calcite, and K-feldspar.

Chemical responses as alteration increases are decreasing MgO and SiO_2 and increasing K_2O, H_2O, and Fe_2O_3/FeO. Calcium oxide ordinarily decreases unless it is fixed as $CaCO_3$ when CO_2 is sufficiently high. Both Al_2O_3 and TiO_2 are relatively immobile, but may increase during extreme alteration due to the removal of other oxides.

TABLE 5
Pyroxene From Holes 417A and 417D

	1	2	3	4	5	6	7	8	9	10	11	12	13	14	15
SiO_2	52.2	52.1	53.0	51.6	51.7	49.9	51.9	51.7	52.5	53.5	51.6	53.0	52.6	47.9	52.0
Al_2O_3	3.23	4.25	2.91	1.61	3.27	3.73	3.94	3.47	2.71	2.09	3.95	3.23	3.53	3.14	1.73
"FeO"	5.99	5.04	7.03	17.7	7.70	10.5	5.62	4.70	6.72	6.17	5.81	3.80	4.84	23.4	22.4
MgO	17.5	17.1	17.3	14.7	17.5	14.6	17.3	17.4	17.7	19.4	17.3	18.1	17.7	8.12	20.6
MnO	0.12	0.17	0.16	0.46	0.19	0.22	0.18	0.16	0.20	0.19	0.16	0.12	0.12	0.77	0.63
TiO_2	0.38	0.31	0.56	0.76	0.66	1.12	0.55	0.43	0.44	0.40	0.69	0.23	0.31	1.88	0.85
Cr_2O_3	0.44	0.80	0.26	0.00	0.62	0.11	0.90	1.20	0.45	0.41	0.92	1.07	0.85	0.15	0.16
CaO	19.3	20.1	19.1	13.8	18.2	18.8	19.6	20.8	19.3	18.0	19.6	21.1	20.6	16.1	3.12
Na_2O	0.16	0.20	0.24	0.14	0.23	0.26	0.21	0.19	0.18	0.11	0.19	0.14	0.17	0.24	0.09
Σ	99.4	100.2	100.6	100.7	100.1	99.2	100.2	100.0	100.2	100.2	100.2	100.8	100.8	101.7	101.4
FeO	5.93	5.04	7.03	17.3	6.64	9.15	5.51	3.61	5.80	6.10	5.36	3.53	4.23	22.0	21.4
Fe_2O_3	0.07	0.00	0.00	0.45	1.17	1.54	0.13	1.21	1.02	0.074	0.502	0.301	0.676	1.57	1.07
Si	1.918	1.897	1.929	1.942	1.894	1.872	1.893	1.886	1.916	1.941	1.883	1.911	1.901	1.857	1.922
Al^{IV}	0.082	0.103	0.071	0.058	0.106	0.128	0.107	0.114	0.084	0.059	0.117	0.089	0.099	0.143	0.075
Σ Tet	2.000	2.000	2.000	2.000	2.000	2.000	2.000	2.000	2.000	2.000	2.000	2.000	2.000	2.000	1.998
Al^{VI}	0.058	0.080	0.054	0.013	0.035	0.037	0.062	0.036	0.032	0.031	0.053	0.048	0.051	0.001	0.000
Fe_2	0.182	0.153	0.214	0.544	0.204	0.287	0.168	0.110	0.177	0.185	0.164	0.106	0.128	0.713	0.662
Fe_3	0.002	0.000	0.000	0.013	0.032	0.044	0.003	0.033	0.028	0.002	0.014	0.008	0.018	0.046	0.030
Mg	0.959	0.929	0.940	0.828	0.957	0.815	0.938	0.945	0.964	1.047	0.940	0.970	0.955	0.469	1.134
Mn	0.004	0.005	0.005	0.015	0.006	0.007	0.006	0.005	0.006	0.006	0.005	0.004	0.004	0.025	0.020
Ti	0.010	0.008	0.015	0.022	0.018	0.032	0.015	0.012	0.012	0.011	0.019	0.006	0.008	0.055	0.024
Cr	0.013	0.023	0.007	0.000	0.018	0.003	0.026	0.035	0.013	0.012	0.027	0.031	0.024	0.005	0.005
Σ Oct	1.227	1.199	1.236	1.433	1.270	1.224	1.218	1.175	1.233	1.293	1.220	1.173	1.189	1.314	1.875
Ca	0.761	0.785	0.745	0.556	0.714	0.757	0.767	0.811	0.754	0.699	0.767	0.817	0.799	0.668	0.124
Na	0.011	0.014	0.017	0.010	0.016	0.019	0.015	0.013	0.013	0.008	0.013	0.010	0.012	0.018	0.006
Total cations	3.999	3.998	3.998	3.999	4.000	4.000	4.000	3.999	4.000	4.000	4.000	4.000	4.000	4.000	4.005
Quad	91.7	88.9	92.3	94.1	89.4	87.2	89.3	88.5	91.5	94.1	88.3	90.7	89.7	85.7	92.4
Others	8.3	11.1	7.6	5.8	10.6	12.8	10.7	11.5	8.5	5.9	11.7	9.3	10.2	14.3	7.5
Quad:															
Wo	40.0	42.0	39.2	28.9	38.1	40.7	40.9	43.5	39.8	36.2	41.0	43.1	42.4	36.1	6.4
En	50.4	49.7	49.5	42.9	51.0	43.8	50.1	50.6	50.9	54.2	50.2	51.2	50.8	25.3	59.1
Fs	9.6	8.2	11.3	28.2	10.9	15.5	9.0	5.9	9.3	9.6	8.7	5.6	6.8	38.5	34.5
Others:															
Ti	10.1	6.8	14.8	23.8	13.0	17.7	11.0	8.5	11.0	14.1	12.6	5.9	7.1	25.4	22.4
NaM2	11.0	11.3	16.4	11.3	11.6	10.6	10.8	9.7	11.7	10.0	9.0	9.3	10.0	8.4	6.1
A14	78.9	82.0	68.8	64.8	75.4	71.7	78.1	81.8	77.3	75.9	78.4	84.8	83.0	66.2	71.5
Best name for others:	CaAl-CaTS	CaAl-CaTS	CaAl-CaTS	CaMg-TAL	CaAl-CaTS	CaMg-TAL	CaAl-CaTS	CaAl-CaTS	CaAl-CaTS	CaAl-CaTS	CaAl-CaTS	CaAl-CaTS	CaAl-CaTS	CaF2-TAL	Mg TAL
$Fe^{2+}/(Fe^{2+}+Mg)$	0.16	0.14	0.19	0.40	0.18	0.26	0.15	0.10	0.16	0.15	0.15	0.10	0.12	0.60	0.37

Note: Column 1: 419D-28-6, 104-110 cm, microphenocryst; Columns 2, 3: 419D-31-2, 93-97 cm, microphenocryst core, rim; Column 4: 419D-33-4, 40-46 cm, groundmass; Column 5: 419D-34-5, 58-64 cm, microphenocryst; Column 6: 419D-34-5, 58-64, groundmass; Column 7: 419D-42-6, 97-102 cm, xenocryst (homogeneous); Column 8: 419D-43-3, 36-42 cm, oikocryst (homogeneous); Column 9: 419D-44-1, 60-66 cm, phenocryst core; Columns 10, 11: 419D-44-4, 80-85 cm, microphenocryst core, rim; Column 12: 419D-55-5, 110-112 cm, glomerocryst; Column 13: 419A-46-1, 23-28 cm, ophitic core; Columns 14, 15: 419A-46-1, 23-28 cm, interstitial quench. Analyses normalized to 6 oxygens. Ferric iron calculated by the method of Papike et al., 1974.

Effects of Alteration on the Rare Earth Elements and Transition Metals

The rare earth elements (REE) and transition metals are important indicators of basalt petrogenesis. Because of this, and because much of the upper part of Layer 2 of the oceanic crust consists of layers of basalt, it is important to understand how these trace elements behave during alteration in the submarine environment. The works of Hart (1969), Hart et al. (1974), Thompson (1973), Frey et al. (1974), and Humphris and Thompson (1978), for example, have provided data on the effects of alteration on selected trace and major elements. In this paper, we are concerned primarily with the effects of low-temperature alteration on the REE and transition metals.

The REE pattern for altered basalt Sample 417A-24-2, 72 cm is parallel to the unaltered samples, but has HREE abundances 20 times that of chondrites, and a small negative Eu anomaly (Figure 5). This overall HREE enrichment may be due either to fractionation of olivine and plagioclase, or to alteration. The severity of the alteration is indicated by its effect on the major elements (Table 1). Depletion of MgO and CaO and enrichment of K_2O and total iron as FeO in this sample are extreme. In spite of this, the rare earth elements (Ce through Yb) maintain geochemical coherency. This contrasts with the conclusions of Ludden and Thompson (1978), based on more extensive data, that alteration significantly changes the abundances of the LREE.

The constant abundances of Zr, Hf, Nb, and Pb between altered samples (e.g., 417A-24-2, 72 cm) and unaltered samples (417A-44-3, 58 cm, and 417D-28-6, 104 cm) indicate that these elements also are essentially unaffected by alteration. Uranium, on the other hand, is significantly en-

TABLE 6
Olivine From Hole 417A

	1	2
SiO_2	39.7	39.0
FeO	12.7	16.2
MnO	0.25	0.37
MgO	46.6	44.1
CaO	0.40	0.40
Cr_2O_3	0.18	0.16
Σ	99.8	100.2
Si	0.992	0.986
Fe	0.264	0.343
Mn	0.005	0.008
Mg	1.731	1.662
Ca	0.011	0.011
Cr	0.004	0.003
Σ	3.007	3.013
FO	86.8	82.9
FA	13.2	17.1

Note: Column 1: 46-1, 23-28 cm, core; Column 2: 46-1, 23-28 cm, rim. Analyses are normalized to 4 oxygens.

TABLE 7
Spinel From Hole 417A

SiO_2	1	2
SiO_2	0.00	0.00
Al_2O_3	27.9	25.6
TiO_2	0.28	0.46
"FeO"	21.7	23.0
MnO	–	0.49
MgO	13.6	13.1
Cr_2O_3	35.7	35.4
Σ	99.1	98.1
Si	0.000	0.000
Al	3.023	2.844
Ti	0.019	0.033
Fe	1.671	1.818
Mn	–	0.039
Mg	1.863	1.847
Cr	2.596	2.643
Fe′ / (Fe′ + Mg)	0.473	0.496

Note: Columns 1, 2: 46-1, 23-28 cm. Analyses normalized to 12 oxygens.

riched in the altered basalt. Furthermore, the Th/U ratio in most Mid-Atlantic Ridge basalts is between 0.9 and 3.3 (Tatsumoto, 1978). This ratio in altered Sample 417A-24-2, 72 cm, is very low at 0.5, which is consistent with an addition of U.

Ba is enriched by a factor of 14 in Sample 417A-24-2, 72 cm, relative to unaltered samples (Table 2, Figure 5). This indicates that Ba also has been introduced during alteration, perhaps by the process suggested by Hart (1969) for large alkali ions.

TABLE 8
Titanomagnetite From Holes 417A and 417D

	1	2	3	4
SiO_2	1.40	0.41	0.00	0.00
Al_2O_3	1.94	1.93	1.60	2.76
TiO_2	22.2	26.4	24.7	23.2
"FeO"	70.5	66.5	72.4	72.0
MnO	0.84	1.79	0.80	0.73
MgO	0.28	0.39	0.23	0.74
Cr_2O_3	0.26	0.27	0.27	0.28
Σ	97.5	97.7	100.0	99.7

Note: Column 1: 417D-33-4, 40-46 cm; Columns 2, 3: 417D-68-2, 67-69; Column 4: 417A-46-1, 23-26.

The transition metals — Sc, Ti, Cr, Mn, Co, and Ni — appear to be immobile during submarine weathering. The altered and unaltered samples are tightly grouped (Figure 6). As noted above, Fe appears to have been added to Sample 417A-24-2, 72 cm. Vanadium in the altered sample is lower by a factor of two than in the unaltered samples.

DISCUSSION

The thick sequence of basalt cooling units in Holes 417A and 417D is characterized by relatively restricted ranges of major element chemistry. Crystal fractionation (of more primitive compositions) as well as alteration account for major element and transition metal abundance variations. Phenocrysts and microphenocrysts of olivine (rarely) or relicts after olivine indicate that it was a liquidus or near liquidus phase in all of our samples. Nickel concentrations (64 to 110 ppm) and $Mg/(Mg + Fe^{2+})$ ratios of 0.55 to 0.65 in the freshest samples are consistent with olivine fractionation prior to emplacement of the magmas.

Olivine was followed in the paragenetic sequence by plagioclase feldspar. This phase played a major role in determining the major element compositional spectrum of the basalts. The variation of MgO and Al_2O_3 (Figure 4) oxides, which are sensitive to olivine and plagioclase fractionation, closely parallels a plagioclase control line. The two natural glasses plot close to the olivine-placioclase cotectic as inferred from abyssal glass compositions (Bence et al., in preparation) and as determined experimentally (Bender et al., in preparation; Fisk, 1978). The crystalline basalts, however, all plot on the plagioclase side of this cotectic. Thus, we have compositional evidence for olivine removal [evolved $Mg/(Mg + Fe^{2+})$ and low Ni] and plagioclase accumulation (high Al_2O_3 relative to MgO). Alumina content might also be affected by mantle heterogeneity, variable degrees of partial melting, or fractionation of minerals other than plagioclase. We reject all of these alternatives on the following grounds: (a) The incompatible trace and minor element abundances do not support a heterogeneous source model; (b) Titania variations, which are much more sensitive to variable degrees of partial melting than alumina, are relatively minor; and (c) Relatively constant Sc and $Mg/(Mg + Fe^{2+})$ ratios are not consistent with variable degrees of

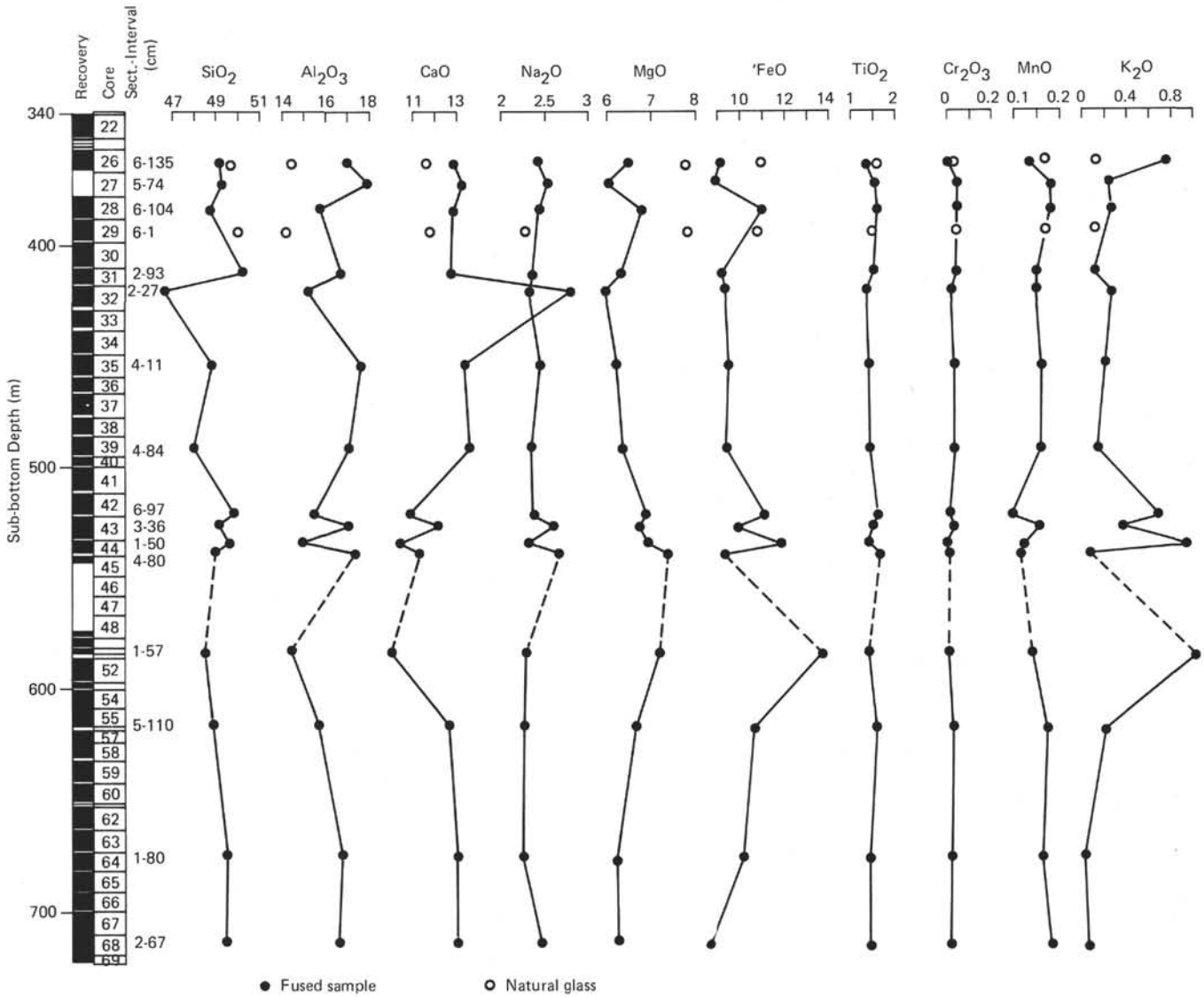

Figure 3. *Chemical variations in Hole 417D basalts.*

clinopyroxene or olivine fractionation. We therefore conclude that the compositional variations in the freshest Hole 417A and 417D basalts are largely a consequence of variable degrees of plagioclase accumulation following olivine fractionation. This accumulation may have been a consequence of flotation in a magma chamber or of flow differentiation at the time of emplacement.

Compositional variations in the plagioclase phenocrysts occurring in the phyric basalts are complex and seem to be consistent with magma mixing. Normal, reversed, and oscillatory zoning in plagioclase phenocrysts from the same thin section is observed. Reversed compositional zoning could be a consequence of a pressure change (P_{total} or P_{H_2O}), but this cannot account for normal zoning in a phenocryst occurring millimeters away. These zoning trends may be reflecting mixing in the magma chamber prior to eruption or in the flow as a consequence of flow turbulence. Although there is evidence that magma mixing occurred, we do not find evidence that it was a fundamental cause of chemical variations in these rocks. If magma mixing was important, either variable parental magmas were extremely well mixed or, more likely, mixing occurred among similar parental magmas in different stages of evolution.

The general similarities of incompatible trace and minor element abundances are consistent with the derivation of all of the Hole 417A and 417D basalts from a homogeneous source region. We contrast this thick sequence of multiple basalt cooling units, all apparently from the same source, with the chemically complex basalt glasses from the Mid-Atlantic rift valley recovered by Project FAMOUS (Langmuir et al., 1977). The striking contrast may reflect different processes of magma generation and eruption at different ridge sites.

The REE patterns of basalts from Holes 417A and 417D have the general characteristics of other "normal" MORBs in that they are light REE depleted with $(La/Yb)_m$ of about 0.6. A significant feature of the isotope dilution REE patterns, however, is the concave downward shape of the heavy REE. This seems to be characteristic of other MORBs with HREE abundances about 15 times that of

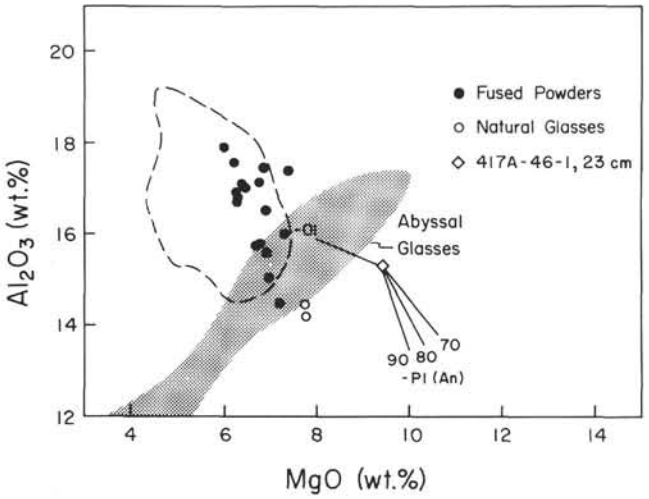

Figure 4. *MgO versus Al_2O_3 diagram for basalts from Holes 417A and 417D. Dashed line indicates field of analyses by Donnelly (1978). Abyssal glass field from Bence et al. (1978). Unfilled circles represent glasses from Hole 417D.*

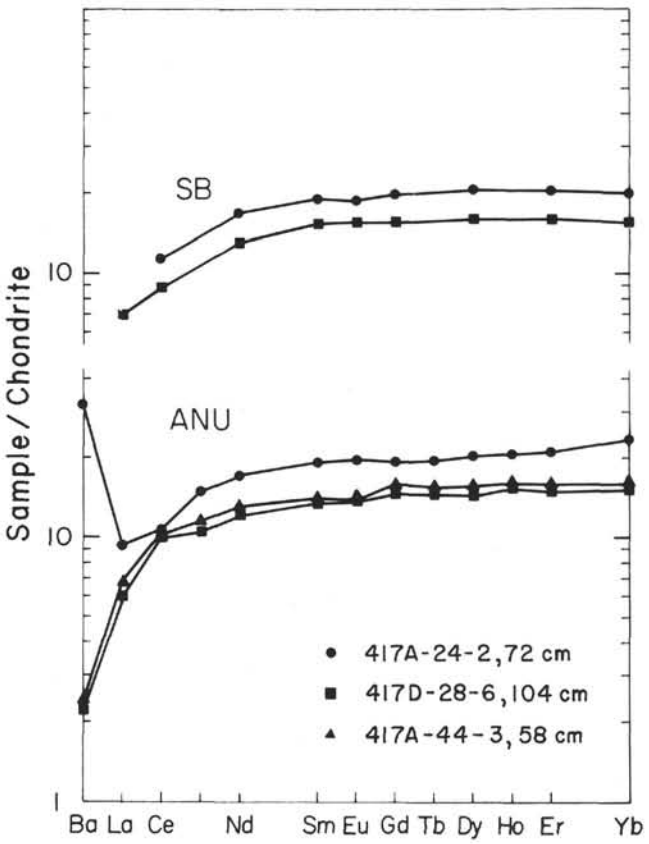

Figure 5. *REE and Ba analyses of selected basalts from Holes 417A and 417D. See text for discussion.*

chondrites, and Al/Ti and Ca/Ti ratios which are significantly less than chondritic (Sun and Nesbitt, 1978). Other LREE-depleted MORBs with HREE abundances about 10 to 12 times that of chondrites tend to have Ca/Ti or Al/Ti

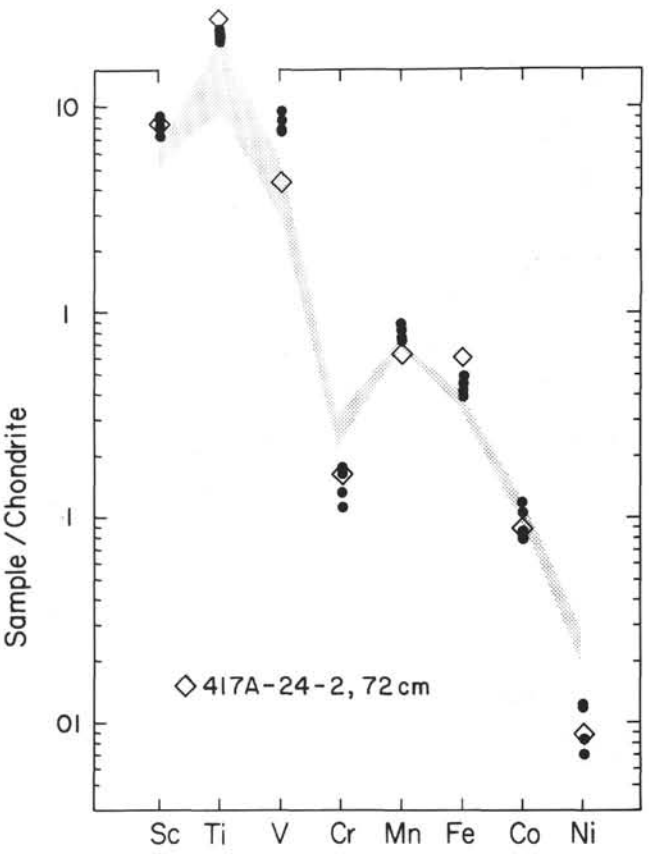

Figure 6. *Transition metal abundances of selected basalts from Holes 417A and 417D. Stippled field encompasses basalt glasses from Project FAMOUS (Langmuir et al., 1977). Sample 417A-24-2, 72 cm is extensively altered.*

ratios which are close to chondritic, and have flat heavy REE, instead of concave downward HREE patterns.

The existence of concave downward HREE patterns may place constraints on the origin of the LREE depletion in the source regions of MORB basalts. There are at least three possible causes for the concave downward shape. Either the shape results from the residual mineralogy left behind for the melting event which gave rise to these basalts, or the shape reflects the source, or some combination of these.

If the source was unfractionated in the HREE relative to chondrites, then a phase must be left behind to retain Yb relative to Gd or Dy. The mantle phases known to do this are garnet and orthopyroxene. However, the evidence from major elements (e.g., Green, 1971) suggests that garnet may not be a residual phase. If the source consisted of 75 per cent olivine and 25 per cent orthopyroxene, then it would require that there be less than 10 per cent melting to fractionate Dy from Yb sufficiently, using the K_d's in Langmuir et al. (1977). Greater degrees of melting would cause too little fractionation of Dy from Yb in the melt. If up to 10 per cent clinopyroxene were present in the residue, then even smaller degrees of melting would be required. For greater than about 10 per cent clinopyroxene, the D for Yb would be smaller than the D for Dy, and no melt could have Dy/Yb greater than the source. So one constraint on the source for the basalts is that *if* the source was unfractionated

in HREE relative to chondrites, and if the K_d's used in the calculations are appropriate, then the basalts were formed by less than 10 per cent melting, and there was less than about 10 per cent clinopyroxene in the source. The larger the amount of clinopyroxene in the source, the lower the degree of partial melting which is required. If these constraints are valid, then the source must have greater than 1.5 times chondritic abundances for the HREE. A way to get around these constraints would be to say that the pyroxene present during melting is neither orthopyroxene nor clinopyroxene, but a subcalcic pyroxene which has K_d's similar in shape to, but larger in magnitude than, those observed in orthopyroxene, as suggested by Sun and Nesbitt (1978).

If the source is not chondritic, then the constraints given above change. If the source has Dy/Yb greater than chondrites, then the constraints on the maximum possible degree of melting and the maximum clinopyroxene contents are relaxed. If, on the other hand, the source has Dy/Yb less than chondrites, then the constraints become even tighter, since Dy must be even more fractionated from Yb than if the source were chondritic. This leads to the question of the origin of the LREE depletion in the source. Gast (1968) and others suggested that the LIL element and LREE depletion was caused by prior melting events. Hanson (1977) has shown, based on K/Rb and K/Ba ratios, that this melting would have to occur under quite specific conditions, with phlogopite retained in the residue for the first melting (which caused the LREE depletion), but not for the second melting (which gave rise to MORBs). We can extend these constraints on the origin of the LREE depletion to garnet. If even a small amount of garnet were present for a first melting event (which caused depletion of the LREE), then the source for the subsequent melting to yield MORB would have Dy/Yb significantly less than chondrites. However, the Dy/Yb ratios of Hole 417A and Hole 417D basalts suggest that the source could not have Dy/Yb less than chondrites unless garnet were retained for the second melting which generated MORBs; this is ruled out by the major elements. Thus, it seems likely that if the LREE depletion in the source was caused by a previous melting event, then garnet was not a residual phase for that melting event, and consequently that that melting event was not one which yielded alkali basalts.

CONCLUSIONS

The following major conclusions arise from this investigation concerning the petrogenesis of basalts from Holes 417A and 417D:

1) The thick sequence of multiple basalt cooling units consists of phyric and ophitic textural types which reflect cooling rate differences.

2) Major element and transition metal abundances indicate that low-pressure fractionation of olivine prior to emplacement and plagioclase accumulation during or after emplacement are responsible for the compositional spectrum of the basalts.

3) Reverse, normal, and oscillatory zoning of the plagioclase phenocrysts within the same sample suggests that magma mixing occurred.

4) Incompatible element abundances suggest a chemically and mineralogically homogeneous source region depleted in the LREE relative to the HREE. If this depletion was caused by a previous melting event of a chondritic source, then garnet was not in the residue for that melting event.

5) Alteration has significantly affected the abundances of SiO_2, MgO, K_2O, H_2O, and Fe_2O_3. Alumina and titania were relatively immobile.

6) In the one highly altered sample which we analyzed, the rare earth elements from Ce to Yb are unfractionated relative to the fresh basalts.

7) Alteration results in the enrichment of Ba and U and the depletion of V. The other transition metals are unaffected.

ACKNOWLEDGMENTS

This research was funded by NSF Grant OCE 7622193AO1 (Submarine Geology and Geophysics). We thank T. W. Donnelly for providing the samples and their major element chemistry prior to publication. The authors are grateful to P. E. Muir and J. M. G. Shelley for analytical determinations.

REFERENCES

Ahrens, L. H. and Taylor, S. R., 1961. *Spectrochemical analysis:* New York (Addison-Wesley).

Ayuso, R. A., Bence, A. E., and Taylor, S. R., 1976. Upper Jurassic tholeiitic basalts from DSDP Leg 11, *J. Geophys. Res.*, v. 81, p. 4305-4325.

Bence, A. E. and Albee, A. L., 1968. Empirical correction factors for the electron microanalysis of silicates and oxides, *J. Geol.*, v. 76, p. 382-403.

Bence, A. E., Papike, J. J., and Ayuso, R. A., 1975. Petrology of submarine basalts from the Central Caribbean: DSDP Leg 15, *J. Geophys. Res.*, v. 80, p. 4775-4804.

Bence, A. E., Baylis, D., and Bender, J. F., in preparation. Major and minor element variations in mid-ocean ridge basalts, Ewing symposium on implications of deep drilling results in the Atlantic Ocean.

Bender, J. F., Hodges, F. N., and Bence, A. E., in preparation. Petrogenesis of basalts from the Project FAMOUS Area: Experimental study from 0Kb to 15 kb.

Bryan, W. B., 1974. Fe-Mg relationships in sector-zoned submarine basalt plagioclase, *Earth Planet. Sci. Lett.*, v. 24, p. 157-165.

Erlank, A. J. and Kable, E. J. D., 1976. The significance of incompatible elements in mid-Atlantic Ridge basalts from 45°N with particular reference to Zr/Nb, *Contrib. Mineral. Petrol.*, v. 54, p. 281-291.

Fisk, M., 1978. Melting relations and mineral chemistry of Iceland and Reykjanes ridge basalts, Ph.D. Thesis, University of Rhode Island.

Frey, F. A., Bryan, W. B., and Thompson, G., 1974. Atlantic ocean floor: Geochemistry and petrology of basalts from legs 2 and 3 of the Deep-Sea Drilling Project, *J. Geophys. Res.*, v. 79, p. 5507-5527.

Gast, P. W., 1968. Trace element fractionation and the origin of tholeiitic and alkaline magma types, *Geochim. Cosmochim. Acta*, v. 32, p. 1057-1086.

Green, D. H., 1971. Composition of basaltic magmas as indicators of conditions of origin: Application to oceanic volcanism, *Phil. Trans. Roy. Soc. London*, Ser. A., v. 268, p. 707-725.

Hanson, G. N., 1977. Geochemical evolution of the suboceanic mantle, *J. Geol. Soc.*, v. 134, p. 235-253.

_____, in preparation. Rare earth element analysis by isotopic dilution, 7th Materials Research Symposium, accuracy in trace analysis (National Bureau of Standards), in press.

Hart, S. R., 1969. K, Rb, Cs contents and K/Rb, K/Cs ratios of fresh and altered submarine basalts, *Earth Planet. Sci. Lett.*, v. 6, p. 295.

Hart, S. R., Erlank, A. J., and Kable, E. J., 1974. Sea floor basalt alteration: some chemical and Sr isotopic effects, *Contrib. Mineral. Petrol.*, v. 44, p. 219-230.

Humphris, S. E. and Thompson, G., 1978. Trace element mobility during hydrothermal alteration of oceanic basalts, *Geochim. Cosmochim. Acta,* v. 42, p. 127-136.

Langmuir, C. H., Bender, J. F., Bence, A. E., Hanson, G. N., and Taylor, S. R., 1977. Petrogenesis of basalts from the FAMOUS area: Mid-Atlantic Ridge, *Earth Planet. Sci. Lett.*, v. 36, p. 133-156.

Ludden, J. N. and Thompson, G., 1978. The modification of the rare earth element abundance of oceanic basalts during low-temperature weathering by seawater, *EOS, Trans. AGU,* v. 59, p. 408.

Mazzulo, L. J. and Bence, A. E., 1976. Abyssal tholeiites from DSDP Leg 34: The Nazca Plate, *J. Geophys. Res.*, v. 81, p. 4327-4351.

Nicholls, I. A., 1974. A direct fusion method of preparing silicate glasses for energy dispersive electron microprobe analysis, *Chem. Geol.*, v. 14, p. 141-157.

Papike, J. J., Cameron, K. L., and Baldwin, K., 1974. Amphiboles and pyroxenes: Characterization of other than quadrilateral components and estimates of ferric iron from microprobe data (abstract), *Geol. Soc. Am. Abstr.* with Programs, v. 6, p. 1053-1054.

Sun, S. S. and Nesbitt, R. W., 1978. Petrogenesis of archean ultrabasic and basic volcanics: Evidence from rare earth elements, *Contrib. Mineral. Petrol.*, v. 65, p. 301-325.

Tatsumoto, M., 1978. Isotopic composition of lead in oceanic basalt and its implication to mantle evolution, *Earth Planet. Sci. Lett.*, v. 38, p. 63-87.

Taylor, S. R. and Gorton, M. P., 1977. Geochemical application of spark source mass spectrometry III, *Geochim. Cosmochim. Acta,* v. 41, p. 1375-1380.

Thompson, G., 1973. A geochemical study of the low-temperature interaction of sea-water and oceanic igneous rocks, *EOS Trans. AGU,* v. 54, p. 1015-1019.

Wagner, L. R. and Brown, G. M., 1967. *Layered igneous rocks:* San Francisco (Oliver and Boyd).

PLATE 1

Figure 1 — Plagioclase phyric basalt, Sample 417D-64-1, 80 cm. Crossed polarizers. Field of view 2.0 × 1.5 mm.

Figure 2 — Subophitic basalt, Sample 417D-68-2, 67 cm. Crossed polarizers. Field of view 2.0 × 1.5 mm.

Figure 3 — Plagioclase glomerocryst in phyric basalt, Sample 417D-67-5, 111 cm. Crossed polarizers. Field of view 2.0 × 1.5 mm.

Figure 4 — Plagioclase-clinopyroxene glomerocryst in phyric basalt, Sample 417-D-42-6, 97 cm. Plane-polarized light. Field of view 2.0 × 1.5 mm.

PLATE 1

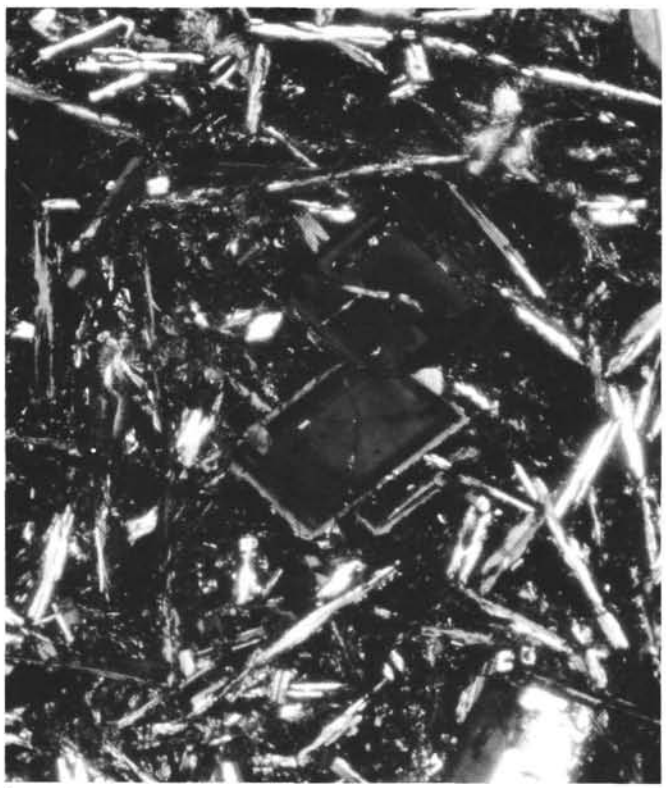

1

2

3

4